Comput. Methods Appl. Mech. Engrg. 267 (2013) 418–433

Contents lists available at ScienceDirect

Comput. Methods Appl. Mech. Engrg.

journal homepage: www.elsevier.com/locate/cma

A family of linearity-preserving schemes for anisotropic diffusion problems on arbitrary polyhedral grids ☆

Weiwei Sun [a], Jiming Wu [b,*], Xiaoping Zhang [c]

[a] Department of Mathematics, City University of Hong Kong, Kowloon, Hong Kong
[b] Institute of Applied Physics and Computational Mathematics, P. O. Box 8009, Beijing 100088, PR China
[c] School of Mathematics and Statistics, Wuhan University, Wuhan 430072, PR China

ARTICLE INFO

Article history:
Received 2 August 2012
Received in revised form 25 January 2013
Accepted 15 August 2013
Available online 11 September 2013

Keywords:
Anisotropic diffusion
Cell-centered scheme
Linearity-preserving criterion
Harmonic averaging point
Polyhedral grids

ABSTRACT

A family of cell-centered finite volume schemes are proposed for anisotropic diffusion problems on arbitrary polyhedral grids with planar facets. The derivation of the schemes is done under a general framework through a certain linearity-preserving approach. The key ingredient of our algorithm is to employ solely the so-called harmonic averaging points located at the cell interfaces to define the auxiliary unknowns, which not only makes the interpolation procedure for auxiliary unknowns simple and positivity-preserving, but also reduces the stencil of the schemes. The final schemes are cell-centered with a small stencil of 25-point on the structured hexahedral grids. Moreover, the schemes satisfy the local conservation condition, treat discontinuity exactly and allow for a simple stability analysis. A second-order accuracy in the L_2 norm and a first-order accuracy in the H_1 norm are observed numerically on general distorted meshes in case that the diffusion tensor is anisotropic and discontinuous.

1. Introduction

In the numerical modelling of many physical problems such as oil reservoir simulations, Lagrangian hydrodynamics with heat and radiative diffusion, Lagrangian magnetohydrodynamics with magnetic diffusion, heat and sweat transfer in porous textile media, diffusion operators are required to be discretized efficiently and robustly on arbitrary distorted polygonal or polyhedral meshes. In many cases, the diffusion coefficient can be an anisotropic or discontinuous tensor, which makes the design of numerical methods for diffusion operators even more difficult.

Up to now, numerous effort has been devoted to developing efficient 2D finite volume schemes for diffusion problems, such as the multi-point flux approximation (MPFA) [1,11,25], the discrete duality finite volume (DDFV) method [18,3,10], the mimetic finite difference (MFD) method [4,23], the gradient scheme [14], the linearity-preserving scheme [26] and the nonlinear monotonic schemes [29,24]. However, these efforts seem not enough in the construction of an ultimate 2D scheme that should possess simultaneously many desirable numerical properties, including small stencil, local conservation, cell-centered primary unknowns, monotonicity, high accuracy on arbitrary distorted grids with an anisotropic and discontinuous diffusion tensor, symmetric positive definite linear system and sound theoretical foundation. The reader is referred to [17] to see some recent achievements in this area. By comparison, the relevant study on 3D grids has drawn less attention.

☆ This work is supported by a grant from City University of Hong Kong (Project No. CityU 102613), the National Natural Science Foundation of China (11271053, 91330205, 11101317) and the Science Foundation of China Academy of Engineering Physics (2011A0202012).

* Corresponding author. Tel.: +86 10 61935090.
E-mail addresses: maweiw@math.cityu.edu.hk (W. Sun), wu_jiming@iapcm.ac.cn (J. Wu), xpzhang.math@whu.edu.cn (X. Zhang).

0045-7825/$ - see front matter © 2013 Elsevier B.V. All rights reserved.
http://dx.doi.org/10.1016/j.cma.2013.08.006

A natural way to construct 3D schemes is to extend the existing 2D schemes. Unfortunately, not all 2D schemes can be easily generalized, since the elements in 3D grids have much more complicated topology relations than their 2D counterparts.

In [19,8,9,20] the DDFV method was generalized to obtain a number of 3D schemes, some of which lead to symmetric positive definite matrices under certain conditions, say, in the case of polyhedral cells having faces with three or four edges. However, the 3D DDFV schemes generally have freedoms or primary unknowns defined at both cell centers and vertices. Through the MFD approach, a family of mixed finite volume schemes were suggested in [4,5] for 3D grids with star-shaped cells. Since the resulting algebraic system in this approach is usually of saddle-point type, the computational cost is an important issue. For this, a cell-centered MFD scheme was then studied in [23] for general polygonal and polyhedral grids, where the resulting linear system is generally non-symmetric. The extension of the MPFA to 3D grids has been studied by several authors. For instance, an MPFA scheme with improved monotonicity was suggested in [6] for arbitrary polyhedral grids. The readers are referred to [12] for some latest developments on 3D finite volume schemes.

By comparison, cell-centered schemes have only one primary unknown for each cell so that they are competitive in some cases, for instance, when a system of coupled differential equations involving diffusion operators are solved on a great number of 3D mesh cells for a long time evolution, e.g., see [22,16] for some examples. Usually, apart from the primary unknowns, almost all cell-centered schemes introduce the so-called auxiliary unknowns which are usually defined on the cell boundaries. These auxiliary unknowns are used only in the construction of the schemes and they are finally eliminated by certain interpolation procedure, whose key ingredient is to express the auxiliary unknowns as linear combinations of the surrounding cell-centered unknowns.

The interpolation procedure is the price that a cell-centered scheme has to pay and it must be done very carefully. A desirable interpolation algorithm should satisfy simultaneously the following properties:

- it is simple and has a local and small stencil;
- it has a second-order accuracy on arbitrary polygonal or polyhedral grids with possibly discontinuous or anisotropic diffusion tensor;
- it is positivity-preserving, i.e., the weights in the linear combination are non-negative.

The third property is probably the most difficult one and it is also one of the key requirements in the construction of certain monotonicity-preserving schemes [29,24]. Most commonly used second-order interpolation algorithms are not positivity-preserving in general, including the MPFA interpolation procedure for edge-centered auxiliary unknowns [21,6,26], the interpolation algorithms of the nine-point scheme and the related linearity-preserving schemes for vertex auxiliary unknowns [30,27,15]. To our knowledge, the only interpolation algorithm that possesses the above three properties is the one based on the so-called harmonic averaging points suggested in [2] and located on cell edges or facets. This interpolation algorithm has a two-point stencil involving two adjacent cells and moreover, the algorithm satisfies the linearity-preserving criterion, i.e., it is exact whenever the exact solution is a linear function on each cell and the diffusion coefficient is a constant on each cell. However, in most cases, the harmonic averaging points do not coincide with the centers of edges or facets and they can be located on the extended parts of the edges or facets, which makes it difficult to design cell-centered schemes using only these special interpolation points. Recently, the harmonic averaging points have been used in [13] to construct a small stencil cell-centered scheme, which has a 27-point stencil in the case of structured hexahedral meshes. In that approach, except for the harmonic averaging points, some extra vertex-based auxiliary unknowns are also introduced.

In this paper, we extend the linearity-preserving approach for 2D girds [26,28] to obtain a family of cell-centered schemes for arbitrary polyhedral grids with possibly discontinuous or anisotropic diffusion tensors. The key ingredient is to use solely the harmonic averaging points to define the auxiliary unknowns, which not only simplifies the interpolation procedure but also reduces the stencil of the schemes. In particular, the new schemes have a 25-point stencil on distorted structured hexahedral meshes. An interesting feature of the new schemes is that the schemes are constructed under a general framework with several parameters. The existence of a family of schemes can be very useful in some cases. For instance, we may search in this family for a specific scheme that has a better performance on accuracy or monotonicity. Another major difference between our schemes with most existing schemes is that the handling of the complex mesh topology around vertices and cell edges in polyhedral grids is completely avoided so that it is almost unnecessary to provide geometric figures to facilitate the description and understanding of our algorithm. The data structures of the mesh topology required in our schemes involve mainly the bilateral relations between cells and facets. Different cells in the same stencil are related through their common facets. Thus, the complexity of implementation of the new schemes in 3D case is almost the same as that of their 2D counterparts and a uniform coding for both 2D and 3D grids becomes possible. One drawback of our schemes could be the nonsymmetry of linear systems. However, this problem can be compensated to some extent since the present approach allows for a simple stability analysis.

The rest of the paper is organized as follows. In Section 2, we state the model problem and introduce some notations. The construction of a family of linearity-preserving schemes is detailed in Sections 3 and 4. The stability analysis of these schemes is given in Section 5. Finally, several numerical experiments are presented in Section 6.

2. Model problem and notations

We consider a diffusion problem on an open bounded polyhedral subset $\Omega \in \mathbb{R}^3$,

$$-\mathrm{div}(\Lambda\nabla u) = f \quad \text{in } \Omega, \tag{2.1}$$

$$u = g_D \quad \text{on } \Gamma_D, \tag{2.2}$$

$$-\Lambda\nabla u\cdot \boldsymbol{n} = g_N \quad \text{on}\,\Gamma_N, \tag{2.3}$$

where $\Lambda(\boldsymbol{x}) : \Omega \to \mathbb{R}^{3\times 3}$ is a symmetric positive definite diffusion tensor, f is the source function, $\partial\Omega = \bar{\Gamma}_D \cup \bar{\Gamma}_N$ is the boundary of Ω, $\boldsymbol{n}$ denotes the outward unit vector normal to the boundary $\partial\Omega$ and $g_D,\ g_N$ are given scalar functions defined on $\Gamma_D,\ \Gamma_N$, respectively.

For the discretization of the domain and the construction of the scheme, we introduce some notations, most of which have been used by some authors and are used here to facilitate the understanding of our algorithm. Throughout this paper, a finite volume discretization of Ω, denoted by $\mathcal{D}$, is defined as the quaternion $\mathcal{D} = (\mathcal{M}, \mathcal{E}, \mathcal{O}, \mathcal{P})$, where.

- $\mathcal{M} = \{K\}$ is a finite family of disjoint open connected polyhedral cells in Ω such that $\bar{\Omega} = \cup_{K\in\mathcal{M}}\bar{K}$. For $K \in \mathcal{M}$, let $\partial K, |K|$ and h_K denote the cell boundary, measure and diameter, respectively. Denote by $h = \max_{K\in\mathcal{M}}\{h_K\}$ the mesh size.
- $\mathcal{E} = \{\sigma\}$ is a finite family of disjoint facets in $\bar{\Omega}$ such that for $\sigma \in \mathcal{E},\ \sigma$ is a planar polygon and has a positive two-dimensional measure denoted as $|\sigma|$. Let $\mathcal{E}^{int} = \mathcal{E}\cap\Omega$ and $\mathcal{E}^{ext} = \mathcal{E}\cap\partial\Omega$. For $K \in \mathcal{M}$, there exists a subset $\mathcal{E}_K$ of $\mathcal{E}$, containing n_K facets, such that $\partial K = \cup_{\sigma\in\mathcal{E}_K}\bar{\sigma}$. $\boldsymbol{n}_{K,\sigma}$ denotes the unit vector normal to $\sigma \in \mathcal{E}_K$ outward to K. In addition, for $\sigma \in \mathcal{E}_K$, notation σ may denote either a generic facet on ∂K or the local number of this same facet in cell K, depending on the context. This slight abuse of notation should not be a source of confusion.
- $\mathcal{O} = \{\boldsymbol{x}_K, K \in \mathcal{M}\}$ is a set of points, known as cell centers, where $\boldsymbol{x}_K \in K$.
- $\mathcal{P} = \cup_{K\in\mathcal{M}}\mathcal{P}_K$, where $\mathcal{P}_K = \{\boldsymbol{x}_{K,\sigma}, \sigma \in \mathcal{E}_K\}$ denotes the set of the interpolation points and $\boldsymbol{x}_{K,\sigma}$ is a point associated with cell K and facet σ.

As for the unknowns, we have the notations below:

- u_K, the primary variable that is the approximation of u at the cell center $\boldsymbol{x}_K$.
- $u_{K,\sigma}$, the intermediate variable that approximates u at the interpolation point $\boldsymbol{x}_{K,\sigma}$.
- $F_{K,\sigma}$, the approximation of the flux $-\int_\sigma(\Lambda_K\nabla u)\cdot\boldsymbol{n}_{K,\sigma}\,ds$, where we assume that Λ is constant on each cell $K \in \mathcal{M}$ with Λ_K denoting the restriction of Λ on K.

Throughout, the hollow letters $\mathbb{A}, \mathbb{F}, \mathbb{X}, \ldots$will be used to denote matrices with column numbers greater than one, while the bold ones $\mathbf{F}, \mathbf{U}, \mathbf{I}, \boldsymbol{n}, \boldsymbol{x}, \ldots$will be employed to denote column vectors.

Finally we introduce a most important notation $\boldsymbol{y}_\sigma$ on which our schemes are based. For an interior facet $\sigma \in \mathcal{E}_K \cap \mathcal{E}_L$, let $\boldsymbol{y}_\sigma$ be defined by

$$\boldsymbol{y}_\sigma = \frac{a_{K,\sigma}\boldsymbol{x}_K + a_{L,\sigma}\boldsymbol{x}_L + \left(\Lambda_K^T - \Lambda_L^T\right)\boldsymbol{n}_{K,\sigma}}{a_{K,\sigma} + a_{L,\sigma}}, \tag{2.4}$$

where

$$a_{K,\sigma} = \frac{\lambda_K^{(n)}}{d_{K,\sigma}}, \quad a_{L,\sigma} = \frac{\lambda_L^{(n)}}{d_{L,\sigma}}, \tag{2.5}$$

$\lambda_K^{(n)} = \boldsymbol{n}_{K,\sigma}^T\Lambda_K\boldsymbol{n}_{K,\sigma},\ \lambda_L^{(n)} = \boldsymbol{n}_{L,\sigma}^T\Lambda_L\boldsymbol{n}_{L,\sigma}$, and $d_{K,\sigma}$ (resp., $d_{L,\sigma}$) denotes the orthogonal distance from $\boldsymbol{x}_K$ (resp., $\boldsymbol{x}_L$) to the hyperplane containing σ.

We introduce the following assumption:

(A1) For any $\sigma \in \mathcal{E}_K \cap \mathcal{E}_L \subset \mathcal{E}$, (i) $\boldsymbol{y}_K - \boldsymbol{x}_K = d_{K,\sigma}\boldsymbol{n}_{K,\sigma}$ and $\boldsymbol{y}_L - \boldsymbol{x}_L = d_{L,\sigma}\boldsymbol{n}_{L,\sigma}$, where $\boldsymbol{y}_K$(resp. $\boldsymbol{y}_L$) is the orthogonal projection point of $\boldsymbol{x}_K$(resp. $\boldsymbol{x}_L$) onto the hyperplane that contains σ; (ii) $\boldsymbol{y}_\sigma \in \bar{\sigma}$. Under assumption (**A1**), we have

$$u(\boldsymbol{y}_\sigma) \simeq \frac{a_{K,\sigma}u(\boldsymbol{x}_K) + a_{L,\sigma}u(\boldsymbol{x}_L)}{a_{K,\sigma} + a_{L,\sigma}}, \tag{2.6}$$

here $\simeq$ is used to indicate that the corresponding relation satisfies the so-called *linearity-preserving criterion* [26,28], i.e., the truncation error vanishes in the linear case where, on any cell $K \in \mathcal{M}$, the solution u is a linear function and at the same time, the diffusion coefficient is a constant tensor. We remark that $\boldsymbol{y}_\sigma$ defined by (2.4) coincides with the so-called *harmonic averaging point* suggested in [2], where the sketch of its derivation on 2D grids was also given. Here, we shall give a different derivation, which holds for both 2D and 3D grids.

As shown in Fig. 1, let $\boldsymbol{y}_\sigma$ be a point on $\bar{\sigma}$ where σ is the common facet of cells K and L in $\mathbb{R}^d$. Let $\boldsymbol{x}_{\sigma,i}(1 \leqslant i \leqslant d)$ be any d vertices of facet σ such that $\boldsymbol{x}_{\sigma,i} - \boldsymbol{x}_{\sigma,1}(2 \leqslant i \leqslant d)$ form an affine coordinate system of the hyperplane containing σ. Due to **(A1)**-(i), we can always write

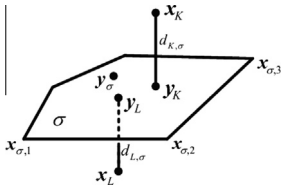

Fig. 1. Notations for the derivation of harmonic averaging point.

$$\begin{aligned}\Lambda_K^T \boldsymbol{n}_{K,\sigma} &= a_{K,\sigma}(\boldsymbol{y}_\sigma - \boldsymbol{x}_K) + \sum_{i=2}^{d} b_{K,i}(\boldsymbol{x}_{\sigma,i} - \boldsymbol{x}_{\sigma,1}),\\ \Lambda_L^T \boldsymbol{n}_{L,\sigma} &= a_{L,\sigma}(\boldsymbol{y}_\sigma - \boldsymbol{x}_L) + \sum_{i=2}^{d} b_{L,i}(\boldsymbol{x}_{\sigma,i} - \boldsymbol{x}_{\sigma,1}),\end{aligned} \tag{2.7}$$

where $a_{K,\sigma}$ and $a_{L,\sigma}$ are given by (2.5), $b_{K,i}$ and $b_{L,i}$ are some constants to be determined. Noting that $\boldsymbol{y}_\sigma \in \bar{\sigma}$, and K and L are simply connected cells, we have

$$\begin{aligned}&u(\boldsymbol{y}_\sigma) - u(\boldsymbol{x}_K) \simeq \bigtriangledown u \cdot (\boldsymbol{y}_\sigma - \boldsymbol{x}_K), \quad u(\boldsymbol{y}_\sigma) - u(\boldsymbol{x}_L) \simeq \bigtriangledown u \cdot (\boldsymbol{y}_\sigma - \boldsymbol{x}_L),\\ &u(\boldsymbol{x}_{\sigma,i}) - u(\boldsymbol{x}_{\sigma,1}) \simeq \bigtriangledown u \cdot (\boldsymbol{x}_{\sigma,i} - \boldsymbol{x}_{\sigma,1}),\ i = 2, \ldots, d.\end{aligned} \tag{2.8}$$

Then, multiplying the two equations in (2.7) with $-\bigtriangledown u$ and integrating on σ, respectively, we have

$$\begin{aligned}\frac{1}{|\sigma|}\int_\sigma (-\Lambda_K \bigtriangledown u)\cdot \boldsymbol{n}_{K,\sigma} ds &\simeq -a_{K,\sigma}(u(\boldsymbol{y}_\sigma) - u(\boldsymbol{x}_K)) - \sum_{i=2}^{d} b_{K,i}(u(\boldsymbol{x}_{\sigma,i}) - u(\boldsymbol{x}_{\sigma,1})),\\ \frac{1}{|\sigma|}\int_\sigma (-\Lambda_L \bigtriangledown u)\cdot \boldsymbol{n}_{L,\sigma} ds &\simeq -a_{L,\sigma}(u(\boldsymbol{y}_\sigma) - u(\boldsymbol{x}_L)) - \sum_{i=2}^{d} b_{L,i}(u(\boldsymbol{x}_{\sigma,i}) - u(\boldsymbol{x}_{\sigma,1})).\end{aligned}$$

By the local conservation condition

$$\int_\sigma (-\Lambda_K \bigtriangledown u)\cdot \boldsymbol{n}_{K,\sigma} ds + \int_\sigma (-\Lambda_L \bigtriangledown u)\cdot \boldsymbol{n}_{L,\sigma} ds = 0,$$

we obtain

$$u(\boldsymbol{y}_\sigma) \simeq \frac{a_{K,\sigma}u(\boldsymbol{x}_K) + a_{L,\sigma}u(\boldsymbol{x}_L)}{a_{K,\sigma} + a_{L,\sigma}} - \sum_{i=2}^{d} \frac{b_{L,i} + b_{K,i}}{a_{K,\sigma} + a_{L,\sigma}}\left[u(\boldsymbol{x}_{\sigma,i}) - u(\boldsymbol{x}_{\sigma,1})\right].$$

Obviously, a sufficient condition for (2.6) is that $b_{K,i} + b_{L,i} = 0 (2 \leqslant i \leqslant d)$. Substituting this condition into (2.7) and noting $\boldsymbol{n}_{K,\sigma} = -\boldsymbol{n}_{L,\sigma}$, we obtain (2.4), which completes the derivation.

By straightforward calculations, we find that

$$(\boldsymbol{y}_\sigma - \boldsymbol{x}_{\sigma,i})\cdot \boldsymbol{n}_{K,\sigma} = 0, \quad 1 \leqslant i \leqslant d,$$

which implies that $\boldsymbol{y}_\sigma$, defined by (2.4), does belong to the hyperplane containing σ.

Remark 2.1. From the above discussion, we can see that the present definition of harmonic averaging point requires that each facet of the polyhedral cells is planar. Therefore, we shall confine the discussion to polyhedral meshes with planar facets. Our method can be developed for polyhedral meshes with non-planar facets in two ways, i.e., by splitting each non-planar facet into planar triangular facets or by following the procedure suggested in [13].

3. A family of linearity-preserving and cell-centered schemes

In this and the next sections, we shall describe in details the construction of a family of linearity-preserving and cell-centered finite volume schemes, which consists of five steps.

3.1. Definition of the primary and auxiliary variables

The primary (resp. auxiliary) variables are defined at the cell centers (resp. interpolation points). Here, the cell center $\boldsymbol{x}_K$ can be the barycenter, the geometric center or any other point in the cell $K \in \mathcal{M}$. As for the interpolation points, we choose $\mathcal{P}_K = \{\boldsymbol{y}_\sigma, \sigma \in \mathcal{E}_K\}$ where, for $\sigma \in \mathcal{E}^{ext}$, $\boldsymbol{y}_\sigma$ is the center of σ; for $\sigma \in \mathcal{E}^{int}$, $\boldsymbol{y}_\sigma$ is defined by (2.4), whether assumption **(A1)** is violated or not. Due to this special choice of $\mathcal{P}_K$, there exists a unique interpolation point associated with each facet, hence we can always write

$$u_{K,\sigma} = u_{L,\sigma} = u_\sigma, \text{ if } \sigma = \mathcal{E}_K \cap \mathcal{E}_L; \quad u_{K,\sigma} = u_\sigma, \text{ if } \sigma \in \mathcal{E}_K \cap \mathcal{E}^{ext}.$$

Here we must point out that assumption **(A1)** just provides a sufficient condition for (2.4) and (2.6). When **(A1)** is violated, it is still possible for us to obtain these two equations. More explicitly, in the case where **(A1)**-(ii) is violated, which is often the case in practice, the whole derivation can still be valid under certain weaker conditions. For example, if $\mathbf{x}_K$ and $\mathbf{y}_\sigma$ (resp. $\mathbf{x}_L$ and $\mathbf{y}_\sigma$) can be connected by a broken line that does not pass through the discontinuities of Λ and $\bigtriangledown u$, then the derivation that follows from (2.8) is still guaranteed. Obviously, alternative conditions of this kind are much weaker than **(A1)**-(ii). Based on these observations, we employ solely the generalized harmonic averaging point $\boldsymbol{y}_\sigma$, defined by (2.4), as interpolation points in the construction of the new cell-centered schemes, which is one of the important characteristics of our method.

3.2. Construction of one-sided flux

For $K \in \mathcal{M}$, once the cell center $\boldsymbol{x}_K$ and the set of interpolation points $\mathcal{P}_K$ are specified, we can establish through some approach, e.g., the linearity-preserving approach in [26,28], the relation below

$$\mathbf{F}_K = \mathbb{A}_K\left(u_K\mathbf{I}_K - \mathbf{U}_K^i\right), \tag{3.1}$$

where $\mathbf{F}_K = (F_{K,\sigma}, \sigma \in \mathcal{E}_K)^T$, $\mathbf{U}_K^i = (u_\sigma, \sigma \in \mathcal{E}_K)^T$, $\mathbf{I}_K$ is an n_K-sized vector with components equal to 1, $\mathbb{A}_K = (a^K_{\sigma,\sigma'})_{n_K \times n_K}$ is referred to as the cell matrix. In order to drive our main idea clear, we have moved the derivation of $\mathbb{A}_K$ to the next section.

3.3. A unique definition of the facet flux

A unique definition of the facet flux is aimed to achieve local conservation. For an interior facet $\sigma \in \mathcal{E}_K \cap \mathcal{E}_L$, we use two one-sided fluxes obtained in the previous step to define

$$\tilde{F}_{K,\sigma} = \mu_{K,\sigma}F_{K,\sigma} - \mu_{L,\sigma}F_{L,\sigma}, \quad \tilde{F}_{L,\sigma} = \mu_{L,\sigma}F_{L,\sigma} - \mu_{K,\sigma}F_{K,\sigma}, \tag{3.2}$$

where $\mu_{K,\sigma}$ and $\mu_{L,\sigma}$ are two positive parameters, satisfying

$$\mu_{K,\sigma} + \mu_{L,\sigma} = 1. \tag{3.3}$$

We remark that any pairs that satisfies the above relation is allowed and the linearity-preserving property is still maintained. Here, we suggest two choices,

$$\mu_{K,\sigma} = \frac{a_{L,\sigma}}{a_{K,\sigma} + a_{L,\sigma}}, \quad \mu_{L,\sigma} = \frac{a_{K,\sigma}}{a_{K,\sigma} + a_{L,\sigma}}, \tag{3.4}$$

$$\mu_{K,\sigma} = \mu_{L,\sigma} = \frac{1}{2}. \tag{3.5}$$

In practice, we prefer to choose the first one, which has been used implicitly in a number of 2D schemes, see, e.g., [26,15,27,28], and facilitates the theoretical analysis.

As for a boundary facet $\sigma \in \mathcal{E}_K \cap \mathcal{E}^{ext}$, we simply set

$$\tilde{F}_{K,\sigma} = \mu_{K,\sigma}F_{K,\sigma} \quad \text{with} \quad \mu_{K,\sigma} = 1. \tag{3.6}$$

Obviously, for the above defined facet fluxes, we have the local conservation condition

$$\tilde{F}_{K,\sigma} + \tilde{F}_{L,\sigma} = 0, \quad \sigma \in \mathcal{E}_K \cap \mathcal{E}_L.$$

3.4. Interpolation of the auxiliary variables

To make the finite volume scheme a cell-centered one, we eliminate the auxiliary variables in the flux expressions by an interpolation procedure. Since we have chosen the (generalized) harmonic averaging points as the interpolation points, the interpolation procedure becomes quite simple and natural. Specifically, we choose the following interpolation formula

$$u_\sigma = \omega_{K,\sigma}u_K + \omega_{L,\sigma}u_L, \quad \sigma \in \mathcal{E}_K \cap \mathcal{E}_L, \tag{3.7}$$

where

$$\omega_{K,\sigma} = \frac{a_{K,\sigma}}{a_{K,\sigma} + a_{L,\sigma}}, \quad \omega_{L,\sigma} = \frac{a_{L,\sigma}}{a_{K,\sigma} + a_{L,\sigma}}. \tag{3.8}$$

By (2.6), (3.7) satisfies the linearity-preserving property if **(A1)** holds. When **(A1)** is violated, interpolation formula (3.7) is still adopted in our schemes, however, its linearity-preserving property may be spoiled.

3.5. The finite volume scheme

With the definition of $\tilde{F}_{K,\sigma}$, we formulate the linearity-preserving and cell-centered finite volume scheme as follows: find the set $\{u_K, K \in \mathcal{M}\}$, such that

$$\sum_{\sigma\in\mathcal{E}_K}\tilde{F}_{K,\sigma} = \int_K f(\boldsymbol{x})\,\mathrm{d}\boldsymbol{x}, \quad \forall\, K \in \mathcal{M}. \tag{3.9}$$

One can see that there exist some undetermined parameters for the general finite volume scheme (3.9), which include $\boldsymbol{x}_K$, $\mathbb{A}_K$ and $\mu_{K,\sigma}$. Once these parameters are specified, a concrete cell-centered finite volume scheme comes out. More interesting is that, thanks to the two-point interpolation formula (3.7), the one-sided flux has a small stencil that involves only cell K and the cells that share a common facet with K. Particularly, for the structured hexahedral meshes, the one-sided flux has a 7-point stencil, which leads to a 25-point stencil for the scheme.

4. Derivation of the cell matrix

Let $\mathbb{F}_K = (f_{\sigma j})$ and $\mathbb{X}_K = (x_{\sigma j})$ be two $n_K \times 3$ matrices, defined by

$$f_{\sigma j} = -|\sigma|\boldsymbol{e}_j^T\Lambda_K^T\boldsymbol{n}_{K,\sigma} \quad \text{and} \quad x_{\sigma j} = \boldsymbol{e}_j^T(\boldsymbol{x}_K - \boldsymbol{y}_\sigma), \tag{4.1}$$

respectively, where $\boldsymbol{e}_1 = (1,0,0)^T$, $\boldsymbol{e}_2 = (0,1,0)^T$, $\boldsymbol{e}_3 = (0,0,1)^T$. By requiring the truncation error of (3.1) to be zero in the linear case and through some straightforward calculations, we have

$$\mathbb{F}_K = \mathbb{A}_K\mathbb{X}_K. \tag{4.2}$$

We point out that any matrix $\mathbb{A}_K$ satisfying (4.2) can be a qualified candidate in our new algorithm. Here, we suggest two approaches.

The first approach, a direct extension of its 2D counterpart [28], is based on the following assumption.

(A2) For any $\sigma \in \mathcal{E}_K (K \in \mathcal{M})$, there exist $\boldsymbol{y}_{i(\sigma)}$, $\boldsymbol{y}_{j(\sigma)}$, $\boldsymbol{y}_{k(\sigma)} \in \mathcal{P}_K$, such that

$$\Lambda_K^T\boldsymbol{n}_{K,\sigma} = \xi_{i(\sigma)}\left(\boldsymbol{y}_{i(\sigma)} - \boldsymbol{x}_K\right) + \xi_{j(\sigma)}\left(\boldsymbol{y}_{j(\sigma)} - \boldsymbol{x}_K\right) + \xi_{k(\sigma)}\left(\boldsymbol{y}_{k(\sigma)} - \boldsymbol{x}_K\right),$$

where

$$\xi_{i(\sigma)} = \frac{\left(\boldsymbol{y}_{j(\sigma)} - \boldsymbol{x}_K, \boldsymbol{y}_{k(\sigma)} - \boldsymbol{x}_K, \Lambda_K^T\boldsymbol{n}_{K,\sigma}\right)}{\left(\boldsymbol{y}_{i(\sigma)} - \boldsymbol{x}_K, \boldsymbol{y}_{j(\sigma)} - \boldsymbol{x}_K, \boldsymbol{y}_{k(\sigma)} - \boldsymbol{x}_K\right)},$$

$$\xi_{j(\sigma)} = \frac{\left(\boldsymbol{y}_{k(\sigma)} - \boldsymbol{x}_K, \boldsymbol{y}_{i(\sigma)} - \boldsymbol{x}_K, \Lambda_K^T\boldsymbol{n}_{K,\sigma}\right)}{\left(\boldsymbol{y}_{i(\sigma)} - \boldsymbol{x}_K, \boldsymbol{y}_{j(\sigma)} - \boldsymbol{x}_K, \boldsymbol{y}_{k(\sigma)} - \boldsymbol{x}_K\right)},$$

$$\xi_{k(\sigma)} = \frac{\left(\boldsymbol{y}_{i(\sigma)} - \boldsymbol{x}_K, \boldsymbol{y}_{j(\sigma)} - \boldsymbol{x}_K, \Lambda_K^T\boldsymbol{n}_{K,\sigma}\right)}{\left(\boldsymbol{y}_{i(\sigma)} - \boldsymbol{x}_K, \boldsymbol{y}_{j(\sigma)} - \boldsymbol{x}_K, \boldsymbol{y}_{k(\sigma)} - \boldsymbol{x}_K\right)},$$

satisfying

$$\xi_{i(\sigma)} \geqslant 0, \ \xi_{j(\sigma)} \geqslant 0, \ \xi_{k(\sigma)} \geqslant 0, \tag{4.3}$$

here $(\boldsymbol{a},\boldsymbol{b},\boldsymbol{c})$ denotes the mixed product of vectors $\boldsymbol{a}$, $\boldsymbol{b}$ and $\boldsymbol{c}$.

The meaning of **(A2)** is that $\boldsymbol{y}_{i(\sigma)} - \boldsymbol{x}_K$, $\boldsymbol{y}_{j(\sigma)} - \boldsymbol{x}_K$ and $\boldsymbol{y}_{k(\sigma)} - \boldsymbol{x}_K$ form an affine coordinates system in space and moreover, $\Lambda_K^T\boldsymbol{n}_{K,\sigma}$ is located in the first quadrant. (4.3) may not be satisfied in certain extreme cases where severe mesh distortion or large anisotropy ratio is presented. In this case, we suggest an alternative choice: find $\boldsymbol{y}_{i(\sigma)}$, $\boldsymbol{y}_{j(\sigma)}$, $\boldsymbol{y}_{k(\sigma)} \in \mathcal{P}_K$, such that the following quantity is maximized,

$$\cos(\mathrm{sgn}(\sigma - i(\sigma))\pi)|\xi_{i(\sigma)}| + \cos(\mathrm{sgn}(\sigma - j(\sigma))\pi)|\xi_{j(\sigma)}| + \cos(\mathrm{sgn}(\sigma - k(\sigma))\pi)|\xi_{k(\sigma)}|. \tag{4.4}$$

Under assumption **(A2)**, we are able to construct a linearity-preserving one-sided flux as follows:

$$F_{K,\sigma} = |\sigma|\left[\xi_{i(\sigma)}\left(u_K - u_{i(\sigma)}\right) + \xi_{j(\sigma)}\left(u_K - u_{j(\sigma)}\right) + \xi_{k(\sigma)}\left(u_K - u_{k(\sigma)}\right)\right]. \tag{4.5}$$

By (4.5) and (3.1), we obtain a desired cell matrix $\mathbb{A}_K$ that respects (4.2).

In the second approach, we suggest a completely new algorithm for $\mathbb{A}_K$. First, we introduce a 3×3 matrix $\mathbb{G}_K$, defined by

$$\mathbb{G}_K = \mathbb{F}_K^T\mathbb{X}_K, \tag{4.6}$$

or equivalently,

$$\mathbb{G}_K = -\Lambda_K^T \sum_{\sigma\in\mathcal{E}_K} |\sigma| \boldsymbol{n}_{K,\sigma} (\boldsymbol{x}_K - \boldsymbol{y}_\sigma)^T. \tag{4.7}$$

When each $\boldsymbol{y}_\sigma$ coincides with the center of the facet σ, by the Stokes formula [14,13], we find that the above definition reduces to

$$\mathbb{G}_K = |K| \Lambda_K^T. \tag{4.8}$$

This same identity can also be found in [4]. However, generally speaking, (4.8) does not hold since the (general) harmonic averaging point $\boldsymbol{y}_\sigma$ may not coincide with the facet centers. Therefore, we need the following assumption for the new approach.

- (**A2′**) For any $K \in \mathcal{M}$, $\mathbb{G}_K$ is invertible.

Under the above assumption, we have the following constructional algorithm for $\mathbb{A}_K$, i.e.,

$$\mathbb{A}_K = \mathbb{F}_K \mathbb{G}_K^{-1} \mathbb{F}_K^T + \mathbb{C}_K^T \mathbb{D}_K \mathbb{C}_K, \tag{4.9}$$

where

$$\mathbb{C}_K = \mathbb{I}_K - \mathbb{X}_K \mathbb{G}_K^{-1} \mathbb{F}_K^T,$$

$\mathbb{I}_K$ is the $n_K \times n_K$ identity matrix and $\mathbb{D}_K$ is an $n_K \times n_K$ arbitrary symmetric positive definite matrix. Obviously, $\mathbb{A}_K$ defined above satisfies (4.2) and the second term in the right-hand side of (4.9) is aimed to improve the stability. In practice, we prefer to choose $\mathbb{D}_K = d\,\mathbb{I}_K$ with $d = O(\kappa(\Lambda_K) h_K)$, where $\kappa(\Lambda_K)$ denotes the condition number of Λ_K.

As can be seen from the above discussion, the constructional algorithm in the second approach fails if $\mathbb{G}_K$ is singular. In our numerical experiments, we have not yet encountered such extreme case. However, theoretical analysis of the invertibility of $\mathbb{G}_K$ is necessary and it seems not so easy for the general polyhedral grids. Here we give some results for $\mathbb{G}_K$ and $\mathbb{A}_K$.

Theorem 4.1. *If all harmonic averaging points associated with K are coplanar, then the matrix $\mathbb{G}_K$, defined by (4.6) or (4.7), is singular. In particular, if K is a tetrahedron with $|K| > 0$, then $\mathbb{G}_K$ is singular if and only if the four harmonic points associated with K are coplanar.*

Proof. Assume that all $\boldsymbol{y}_\sigma (\sigma \in \mathcal{E}_K)$ associated with K are located in a plane whose normal vector is denoted as $\boldsymbol{v}$. Then, we have

$$(\boldsymbol{y}_\sigma - \boldsymbol{y}_{\sigma'})^T \boldsymbol{v} = 0, \quad \forall\, \sigma, \sigma' \in \mathcal{E}_K. \tag{4.10}$$

By (4.7) and the identity $\sum_{\sigma\in\mathcal{E}_K} |\sigma| \boldsymbol{n}_{K,\sigma} = \boldsymbol{0}$ with $\boldsymbol{0} \in \mathbb{R}^3$ denoting the zero vector, we have

$$\mathbb{G}_K \boldsymbol{v} = -\Lambda_K \sum_{\sigma\in\mathcal{E}_K} |\sigma| (\boldsymbol{x}_K^T \boldsymbol{v} - \boldsymbol{y}_\sigma^T \boldsymbol{v}) \boldsymbol{n}_{K,\sigma} = \Lambda_K \sum_{\sigma\in\mathcal{E}_K} |\sigma| (\boldsymbol{y}_\sigma^T \boldsymbol{v} - \boldsymbol{y}_{\sigma'}^T \boldsymbol{v}) \boldsymbol{n}_{K,\sigma} = \boldsymbol{0}, \tag{4.11}$$

which implies that $\mathbb{G}_K$ is singular. Now, assume that K is a tetrahedron and $\mathbb{G}_K$ is singular, then there exists a non-trivial vector $\boldsymbol{v}$ such that $\mathbb{G}_K \boldsymbol{v} = 0$. By (4.11) and by recalling that Λ_K is symmetric positive definite, we have

$$\sum_{\sigma\in\mathcal{E}_K, \sigma\neq\sigma'} |\sigma| (\boldsymbol{y}_\sigma^T \boldsymbol{v} - \boldsymbol{y}_{\sigma'}^T \boldsymbol{v}) \boldsymbol{n}_{K,\sigma} = \boldsymbol{0}, \quad \forall\, \sigma' \in \mathcal{E}_K. \tag{4.12}$$

The assumption $|K| > 0$ implies that the three vectors $\boldsymbol{n}_{K,\sigma}, \sigma \in \mathcal{E}_K, \sigma \neq \sigma'$, are linearly independent. As a result, we deduce from (4.12) that

$$\boldsymbol{y}_\sigma^T \boldsymbol{v} - \boldsymbol{y}_{\sigma'}^T \boldsymbol{v} = 0, \quad \forall\, \sigma, \sigma' \in \mathcal{E}_K, \tag{4.13}$$

which implies that the four harmonic averaging points associated with K are coplanar. The proof is complete. □

Theorem 4.2. *If the symmetric part of $\mathbb{G}_K^{-1}$ is positive definite, then for the cell matrix $\mathbb{A}_K$ defined by (4.9), we have*

$$\boldsymbol{v}^T (\mathbb{A}_K + \mathbb{A}_K^T) \boldsymbol{v} > 0, \tag{4.14}$$

where $\boldsymbol{v}$ is any none-zero vector in $\mathbb{R}^{n_K}$.

Proof. For any $\boldsymbol{v} \in \mathbb{R}^{n_K}$, we have

$$\boldsymbol{v}^T (\mathbb{A}_K + \mathbb{A}_K^T) \boldsymbol{v} = \boldsymbol{v}^T \mathbb{F}_K (\mathbb{G}_K^{-1} + \mathbb{G}_K^{-T}) \mathbb{F}_K^T \boldsymbol{v} + 2 \boldsymbol{v}^T \mathbb{C}_K^T \mathbb{D}_K \mathbb{C}_K \boldsymbol{v} \geqslant 0,$$

where we have used the facts that the symmetric part of $\mathbb{G}_K^{-1}$ is positive definite and $\mathbb{D}_K$ is symmetric positive definite. If there exists $\boldsymbol{v} \in \mathbb{R}^{n_K}$ such that $\boldsymbol{v}^T(\mathbb{A}_K + \mathbb{A}_K^T)\boldsymbol{v} = 0$, then

$$\mathbb{F}_K^T \boldsymbol{v} = 0 \quad \text{and} \quad \mathbb{C}_K \boldsymbol{v} = (\mathbb{I}_K - \mathbb{X}_K \mathbb{G}_K^{-1} \mathbb{F}_K^T)\boldsymbol{v} = 0,$$

which implies $\boldsymbol{v} = 0$ and completes the proof. □

5. Stability analysis

The linearity-preserving schemes discussed in the previous sections are generally non-symmetric. The stability of schemes of this type is an important issue, which will be investigated here through a discrete functional approach. For simplicity, throughout this section, we shall just consider the case where (3.4) is employed in the unique definition of the facet flux and a pure and homogeneous Dirichlet boundary condition is imposed on $\partial\Omega$. Analysis for a more general case can be done in almost the same way but involves some tedious details.

We first introduce some notations and assumptions that will be used in the analysis.

- $X(\mathcal{M})$ denotes the set of discrete functions that have constant values on each element of $\mathcal{M}$;
- $\mathbb{Q}_K$ is an $n_K \times n_K$ diagonal matrix whose σ-th diagonal entry is $|\sigma|/d_\sigma$, where $d_\sigma = d_{K,\sigma} + d_{L,\sigma}$ if $\sigma = \mathcal{E}_K \cap \mathcal{E}_L$ and $d_\sigma = d_{K,\sigma}$ if $\sigma \in \mathcal{E}_K \cap \mathcal{E}^{ext}$;
- $\mathbb{M}_K$ is an $n_K \times n_K$ diagonal matrix whose σ-th diagonal entry is $\mu_{K,\sigma}$;
- $\mathbf{U}_K^c$ denotes an n_K-sized vector, whose σ-th component is u_L if $\sigma = \mathcal{E}_K \cap \mathcal{E}_L$ and vanishes if $\sigma \in \mathcal{E}^{ext}$.

For $u_\mathcal{M} = \{u_K, K \in \mathcal{M}\} \in X(\mathcal{M})$, its discrete L_2 and H_1 norms are defined by

$$\|u_\mathcal{M}\|_{0,\mathcal{M}} = \left(\sum_{K\in\mathcal{M}} |K| u_K^2\right)^{1/2}, \tag{5.1}$$

$$\|u_\mathcal{M}\|_{1,\mathcal{M}} = \left(\sum_{K\in\mathcal{M}} \|\mathbb{Q}_K^{1/2}(u_K \mathbf{I}_K - \mathbf{U}_K^c)\|^2\right)^{1/2}, \tag{5.2}$$

respectively. In addition, we introduce the following assumptions:

- (**A3**) For the finite volume discretization $\mathcal{D} = (\mathcal{M}, \mathcal{E}, \mathcal{O}, \mathcal{P})$, there exist constants α, β and γ, such that

  $$|K| \geqslant \alpha h^3, \ n_K \leqslant \gamma, \ \forall K \in \mathcal{M} \quad \text{and} \quad |\sigma| \geqslant \beta h^2, \ \forall \sigma \in \mathcal{E};$$

- (**A4**) There exists a positive constant $\overline{q}$, independent of K, σ and h, such that

  $$\frac{|\sigma|}{d_\sigma} \leqslant \overline{q} h, \quad \forall \sigma \in \mathcal{E}_K, \quad \forall K \in \mathcal{M};$$

- (**A5**) There exists a positive constant σ_K, independent of h, such that

  $$\frac{1}{2}\boldsymbol{v}^T(\mathbb{A}_K + \mathbb{A}_K^T)\boldsymbol{v} \geqslant \sigma_K h \|\boldsymbol{v}\|^2, \quad \forall \ \boldsymbol{v} \in \mathbb{R}^{n_K}, \quad \forall K \in \mathcal{M}. \tag{5.3}$$

Now we are ready to do the stability analysis.

Theorem 5.1. *Let $u_\mathcal{M} = \{u_K, K \in \mathcal{M}\} \in X(\mathcal{M})$ be the solution of the finite volume scheme suggested in Sections 3 and 4. Assume that $\Gamma_D = \partial\Omega$, $g_D = 0$, $\mu_{K,\sigma}$ is given by (3.4) and all cell matrices $\mathbb{A}_K$ can be constructed out. Then under assumptions (**A3**)–(**A5**), we have*

$$\|u_\mathcal{M}\|_{1,\mathcal{M}} \leqslant \frac{C_P\, \overline{q}}{\min\limits_{\sigma\in\mathcal{E}_K, K\in\mathcal{M}}\{\sigma_K \mu_{K,\sigma}^2\}} \|f\|_{0,\Omega}, \tag{5.4}$$

where $\|\cdot\|_{0,\Omega}$ denotes the standard L_2 norm, and C_P is a constant defined in (5.6).

Proof. First, multiplying both sides of (3.9) with u_K, summing over all cells in $\mathcal{M}$ and using the Cauchy-Schwartz inequality, we have

$$\sum_{K\in\mathcal{M}}\sum_{\sigma\in\mathcal{E}_K} u_K \tilde{F}_{K,\sigma} = \sum_{K\in\mathcal{M}} u_K \int_K f(\boldsymbol{x})d\boldsymbol{x} \leqslant \|u_\mathcal{M}\|_{0,\mathcal{M}} \|f\|_{0,\Omega}. \tag{5.5}$$

Under assumption (**A3**), we have the discrete Poincaré inequality,

$$\|u_{\mathcal{M}}\|_{0,\mathcal{M}} \leqslant C_P \|u_{\mathcal{M}}\|_{1,\mathcal{M}}, \tag{5.6}$$

where C_P is a positive constant, possibly dependent on α, β and γ, and independent of $u_{\mathcal{M}}$ and h. The proof of this inequality is essentially the same as that of its 2D counterpart (see, e.g., Lemma 5.1 in [7]) and is therefore omitted for simplicity. From (5.5) and (5.6), we have

$$\sum_{K\in\mathcal{M}}\sum_{\sigma\in\mathcal{E}_K} u_K \tilde{F}_{K,\sigma} \leqslant C_P \|u_{\mathcal{M}}\|_{1,\mathcal{M}} \|f\|_{0,\Omega}. \tag{5.7}$$

Secondly, for an interior facet $\sigma \in \mathcal{E}_K \cap \mathcal{E}_L$, we deduce from (3.7), (3.8) and (3.4) that

$$u_\sigma = \mu_{K,\sigma} u_L + (1-\mu_{K,\sigma}) u_K.$$

For a boundary facet $\sigma \in \mathcal{E}_K \cap \mathcal{E}^{ext}$, $\mu_{K,\sigma} = 1$ and $u_\sigma = 0$. Then we have

$$\mathbf{U}_K^i = \mathbb{M}_K \mathbf{U}_K^c + u_K(\mathbf{I}_K - \mathbb{M}_K \mathbf{I}_K). \tag{5.8}$$

Substituting this equation into (3.1) yields

$$\mathbf{F}_K = \mathbb{A}_K \mathbb{M}_K (u_K \mathbf{I}_K - \mathbf{U}_K^c). \tag{5.9}$$

By (3.2), (3.6) and (5.9), we have

$$\begin{aligned}\sum_{K\in\mathcal{M}}\sum_{\sigma\in\mathcal{E}_K} u_K \tilde{F}_{K,\sigma} &= \sum_{K\in\mathcal{M}} \left(\sum_{\sigma\in\mathcal{E}_K\cap\mathcal{E}_L} (u_K - u_L)\mu_{K,\sigma} F_{K,\sigma} + \sum_{\sigma\in\mathcal{E}_K\cap\mathcal{E}^{ext}} u_K \mu_{K,\sigma} F_{K,\sigma} \right) = \sum_{K\in\mathcal{M}} (u_K \mathbf{I}_K - \mathbf{U}_K^c)^T \mathbb{M}_K \mathbf{F}_K \\ &= \frac{1}{2} \sum_{K\in\mathcal{M}} (u_K \mathbf{I}_K - \mathbf{U}_K^c)^T \mathbb{M}_K (\mathbb{A}_K + \mathbb{A}_K^T) \mathbb{M}_K (u_K \mathbf{I}_K - \mathbf{U}_K^c).\end{aligned}$$

Finally, by assumptions (**A4**) and (**A5**), we conclude that

$$\sum_{K\in\mathcal{M}}\sum_{\sigma\in\mathcal{E}_K} u_K \tilde{F}_{K,\sigma} \geqslant \sum_{K\in\mathcal{M}} \sigma_K h \|\mathbb{M}_K (u_K \mathbf{I}_K - \mathbf{U}_K^c)\|^2 \geqslant \frac{1}{\bar{q}} \min_{\sigma\in\mathcal{E}_K, K\in\mathcal{M}} \{\sigma_K \mu_{K,\sigma}^2\} \sum_{K\in\mathcal{M}} \|\mathbb{Q}_K^{1/2} (u_K \mathbf{I}_K - \mathbf{U}_K^c)\|^2 = \frac{1}{\bar{q}} \min_{\sigma\in\mathcal{E}_K, K\in\mathcal{M}} \{\sigma_K \mu_{K,\sigma}^2\} \|u_{\mathcal{M}}\|_{1,\mathcal{M}}^2.$$

Combining this with (5.7), we obtain (5.4), which completes the proof. □

6. Numerical examples

In this section, we present some numerical results to demonstrate the efficiency and robustness of the linearity-preserving schemes discussed in the previous sections. We first describe the schemes, meshes, notations and assumptions used in the numerical tests. The concrete schemes investigated in this section are described in Table 1. As for the meshes, we recall that, in the sixth conference on finite volumes for complex applications (FVCA VI for short), some existing schemes were compared on six typical types of polyhedral meshes with planar facets [12]. Here, we shall employ all six mesh types to test our schemes, see Table 2 and Fig. 2 for descriptions and examples of the meshes, where the subscripts represent the mesh levels. All mesh data are downloaded from a web site of FVCA VI at the following URL: `http://www.latp.univ-mrs.fr/latp_numerique/?q=node/4`.

We have seen from the above sections that our schemes employ solely the harmonic averaging points to define auxiliary unknowns. So, the violation of assumption **(A1)**, which reduces to $\boldsymbol{y}_\sigma \notin \bar{\sigma}$ in most cases, is an important issue and it should be investigated intensively. For this purpose, we introduce the following notations:

- $v(\sigma) = \min_{\boldsymbol{x}\in\bar{\sigma}} |\boldsymbol{x} - \boldsymbol{y}_\sigma|/h$, denoting the normalized distance from the harmonic averaging point $\boldsymbol{y}_\sigma$ to the closed enclosure of facet σ;
- v_{max}: the maximal value of $v(\sigma)$ over the set $\{\sigma : \boldsymbol{y}_\sigma \notin \bar{\sigma}\}$;
- $\bar{v}$: the simple average of $v(\sigma)$ over the set $\{\sigma : \boldsymbol{y}_\sigma \notin \bar{\sigma}\}$;
- `pval`: percentage for violation of assumption **(A1)**.

Table 1
Schemes investigated in the numerical tests.

Scheme	$\boldsymbol{x}_K$	$\mathbb{A}_K$	$\mu_{K,\sigma}$
LPS-1	geometric center	(4.5) and (3.1)	(3.4)
LPS-2	geometric center	(4.5) and (3.1)	(3.5)
LPS-3	geometric center	(4.9)	(3.4)

Table 2
Meshes with planar facets used in the numerical tests.

Generic name	Description	Level	Provider
Mesh B_i	Tetrahedral meshes	$1 \leqslant i \leqslant 6$	F. Hubert
Mesh C_i	Voronoi meshes	$1 \leqslant i \leqslant 5$	G. Manzini
Mesh D_i	Kershaw meshes	$1 \leqslant i \leqslant 4$	K. Lipnikov
Mesh F_i	Prism meshes with general bases	$1 \leqslant i \leqslant 4$	G. Manzini
Mesh H_i	Locally refined hexahedral meshes	$1 \leqslant i \leqslant 5$	S. Minjeaud
Mesh I_i	Checkerboard meshes	$1 \leqslant i \leqslant 5$	S. Minjeaud

Throughout, all tests are performed in double precision, and BICGSTAB is used to solve linear systems with stoping tolerance ε_{lin}=1.0E-10. In addition, the notations below will be used in the numerical tests.

- `nunkw`: number of primary unknowns;
- `ms`: maximal stencil that equals to the maximal number of non-zero row entries of the coefficient matrix;
- `as`: averaging stencil that equals to the ratio between the total number of non-zero entries in the coefficient matrix and the number of primary unknowns;
- `umin`: minimal value of the approximate solution;
- `umax`: maximal value of the approximate solution.

6.1. Test 1: mild anisotropic problem

First we solve the problem (2.1) and (2.2) on the cubic domain $\Omega = [0,1]^3$. The diffusion tensor and exact solution are given respectively by

$$\Lambda_1 = \begin{pmatrix} 1 & 0.5 & 0 \\ 0.5 & 1 & 0.5 \\ 0 & 0.5 & 1 \end{pmatrix}, \quad u_1(x,y,z) = 1 + \sin(\pi x)\sin\left(\pi\left(y+\frac{1}{2}\right)\right)\sin\left(\pi\left(z+\frac{1}{3}\right)\right),$$

where $u_1(x,y,z)$ is located in the interval $[0,2]$. This test comes from [12].We first test our schemes on the unstructured tetrahedral meshes (Mesh B_1 - Mesh B_6).

Some detailed data concerning the numerical performance of the three schemes are presented in Table 3 where `nunkw`, `ms`, `as`, `pval`, v_{max} and $\bar{v}$ are presented respectively in a single row since they are the same for three schemes. One can see that three schemes have a 17-point stencil for these tetrahedral meshes. We observe from the table that there do exist a few cases where assumption **(A1)** is violated and the distance from the harmonic averaging point to the cell facet seems to be $O(h)$, however, the numerical results are still satisfactory and competitive with those in [12]. As for the monotonicity, all three schemes respect the physical bounds in this test, although they are not designed to be monotonicity-preserving ones. The L_2 and H_1 errors are also graphically presented as log–log plots of errors versus the mesh size h in Fig. 3, where approximately second order accuracy for the L_2 errors and first order accuracy for the H_1 errors for three schemes can be explicitly observed.

We then solve this same problem on the rest five mesh types and some main results for all six mesh types are summarized in Table 4, where.

- `nunkw`, `ms`, `as`, `pval`, v_{max} and $\bar{v}$ are given for the last mesh level;
- `umin` and `umax` are given for the first mesh level;
- L_2 and H_1 error orders are obtained from all meshes of the same type though a least squares fit.

From Table 4 we can see that three schemes have good numerical performance over most mesh types except Mesh D, the 3D Kershaw mesh. By comparison, the L_2 and H_1 error orders of LPS3 are much better than those of LPS1 and LPS2, while LPS1 and LPS2 have much better monotonicity performance than LPS3.

6.2. Test 2: strong anisotropic problem

In this test, we solve the diffusion Eqs. (2.1) and (2.2) on $[0,1]^3$ with diffusion tensors given by

$$\Lambda_2 = \mathrm{diag}(1,1,100) \quad \text{and} \quad \Lambda_3 = \mathrm{diag}(1,1,1000),$$

respectively. The right-hand side function and the Dirichlet boundary data are determined by the exact solution

$$u_2(x,y,z) = \sin(\pi x)\sin(\pi y)\sin(\pi z).$$

This problem is taken from [13].

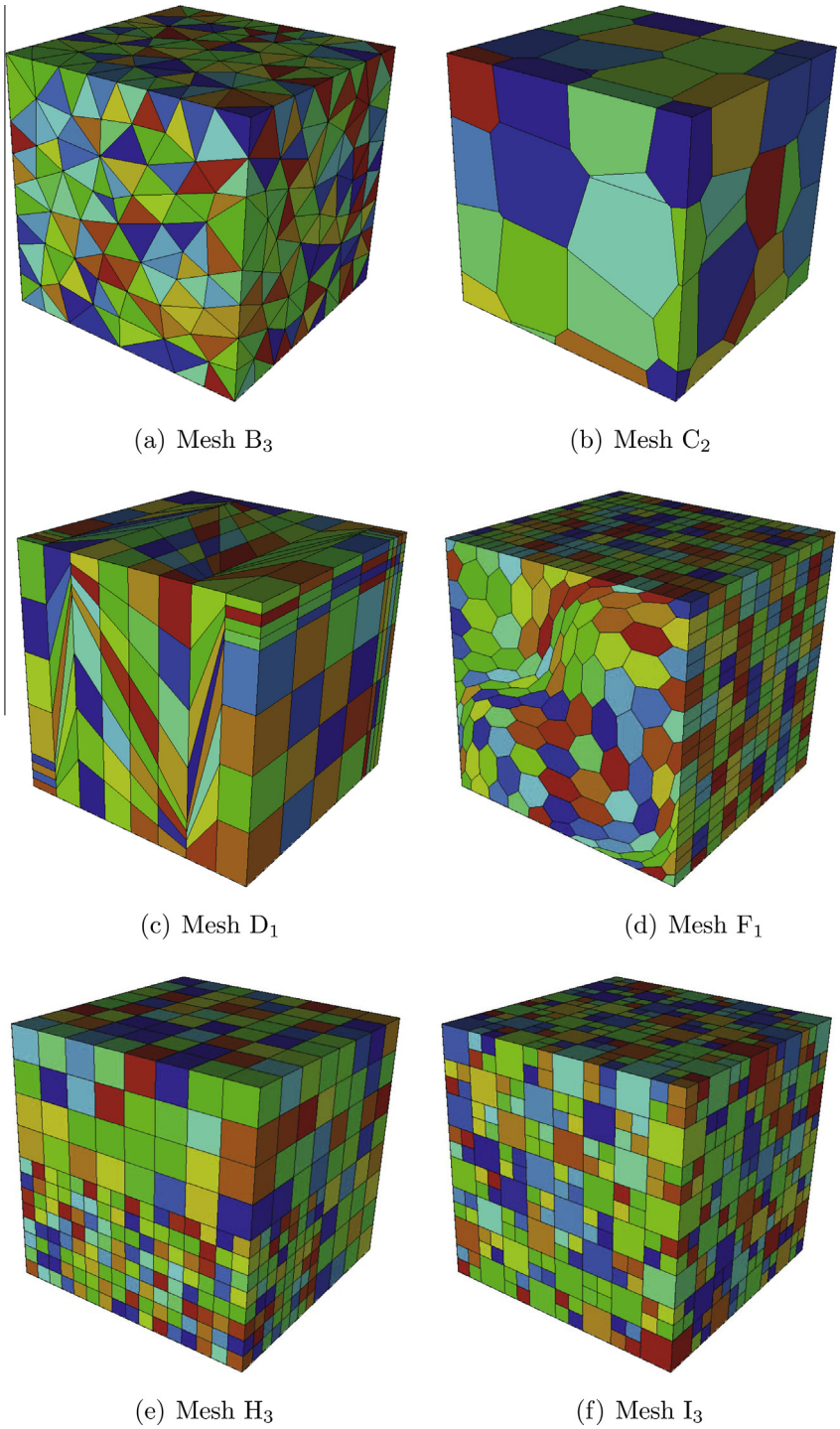

Fig. 2. Examples of the polyhedral meshes with planar facets.

We first use the aforementioned six mesh types to test our schemes. The numerical results with respect to Λ_3 are presented in Table 5 where `nunkw`, `ms`, `as`, `pval`, v_{max} and $\bar{v}$ are deleted since they are the same as those in Table 4. One can see that the numerical performance of three schemes is similar to Test 1 except that the error orders on Mesh D are much improved while those on Mesh B become worse. Here we point out that LPS1 and LPS2 fail on the finest mesh level of Mesh I due to the failure of BICGSTAB in this strongly anisotropic case.

As pointed out before, our linearity-preserving schemes are mainly designed for polyhedral meshes with planar facets. For polygonal meshes with non-planar facets, there is a simple technique that makes our schemes still available in such

Table 3
Numerical results for Λ_1 on unstructured tetrahedral meshes.

Item	Scheme	Mesh B_1	Mesh B_2	Mesh B_3	Mesh B_4	Mesh B_5	Mesh B_6
nunkw		44	215	2003	3898	7711	15266
ms		16	17	17	17	17	17
as		9.45	11.47	13.54	13.89	14.13	14.36
pval		0.00%	1.20%	1.49%	1.27%	1.22%	1.34%
v_{max}		–	3.48e−2	7.17e−2	6.27e−2	5.21e−2	7.39e−2
$\bar{v}$		–	1.36e−2	1.46e−2	1.67e−2	1.32e−2	1.52e−2
umin	LPS-1	1.70e−1	5.85e−2	3.60e−2	1.07e−2	1.56e−2	9.87e−3
	LPS-2	1.72e−1	5.98e−2	3.49e−2	1.33e−2	1.57e−2	9.42e−3
	LPS-3	9.98e−2	2.22e−2	2.00e−2	3.37e−3	7.93e−3	4.45e−3
umax	LPS-1	1.7494	1.9188	1.9759	1.9783	1.9890	1.9920
	LPS-2	1.7477	1.9188	1.9690	1.9790	1.9894	1.9923
	LPS-3	1.8594	1.9785	1.9874	1.9911	1.9989	1.9975
$L_2 - error$	LPS-1	6.37e−2	2.92e−2	8.58e−3	6.22e−3	3.70e−3	2.47e−3
	LPS-2	6.27e−2	2.83e−2	8.43e−3	6.22e−3	3.71e−3	2.45e−3
	LPS-3	5.96e−2	2.49e−2	5.93e−3	4.03e−3	2.59e−3	1.63e−3
$H_1 - error$	LPS-1	5.64e−1	5.05e−1	2.53e−1	2.05e−1	1.55e−1	1.28e−1
	LPS-2	5.77e−1	4.73e−1	2.41e−1	1.98e−1	1.50e−1	1.30e−1
	LPS-3	6.26e−1	4.73e−1	2.27e−1	1.81e−1	1.41e−1	1.13e−1

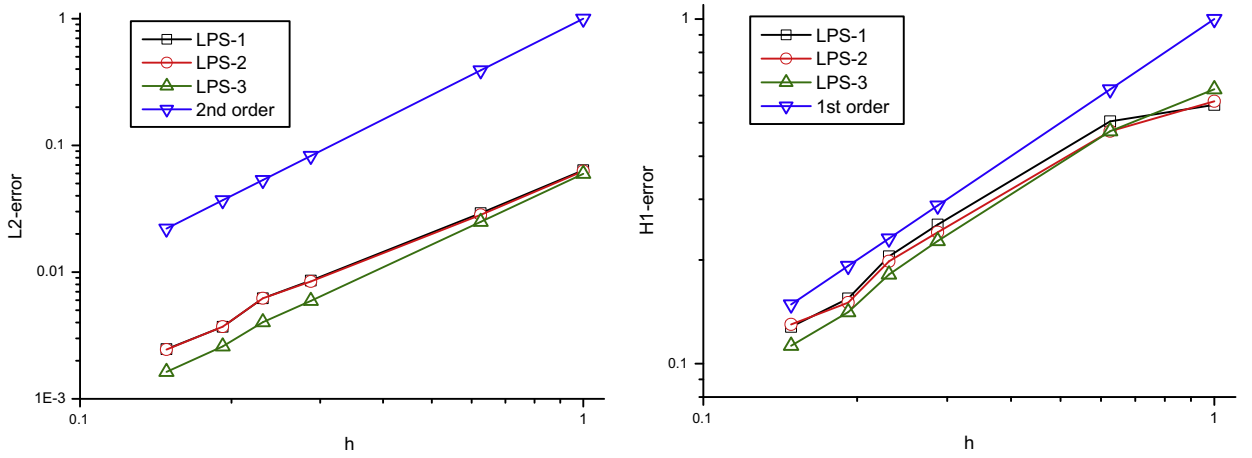

Fig. 3. Test 1: errors for Λ_1 on unstructured tetrahedral meshes.

cases. We simply split each non-planar facet into triangular facets. This technique has no influence on the stencil of our schemes and moreover, the rest implementation is the same as that of the planar facet case. Here we employ a sequence of randomly disturbed hexahedral meshes (Mesh AA_1 - Mesh AA_4), which are also downloaded at the URL: `http://www.latp.univ-mrs.fr/latp_numerique/?q=node/4`. These meshes are generated by randomly disturbing the vertices of corresponding uniform cubic meshes, see Fig. 4 for two examples of such meshes. Since all the vertices, including those on the boundary, are randomly disturbed in three directions, nearly all the facets are now non-planar quadrilaterals. In this case, we split each non-planar quadrilateral facet into two triangular facets. The definition of the harmonic averaging points and the examination of violation of assumption **(A1)** are done with respect to these newly generated triangular facets, instead of the original non-planar facets. Numerical results are given in Table 6 and Table 7, respectively. The data for nunkw, ms, as, pval, v_{max} and $\bar{v}$ are deleted from Table 7 since they are almost the same as those in Table 6. One can see that our schemes have a 25-point stencil in this case. In addition, LPS-3 respects physical bounds in this test while the rest two exhibit good monotonicity on coarse meshes. The errors as functions of the mesh size h for Λ_2 and Λ_3 are depicted in Figs. 5 and 6, respectively. It is interesting to note that the L_2 (resp. H_1) error has approximately second (resp. first) order accuracy for both Λ_2 and Λ_3, although the rates of violation of **(A1)** are very high.

6.3. Test 3: discontinuous anisotropic problem

Now we solve (2.1) on $[0,1]^3$ with the full Dirichlet boundary condition and a discontinuous and anisotropic diffusion tensor. The diffusion tensor and the exact solution are given by

Table 4
Numerical results for Λ_1 on all six mesh types.

Item	Scheme	Mesh B	Mesh C	Mesh D	Mesh F	Mesh H	Mesh I
nunkw		15266	356	262144	67240	90112	147456
ms		17	99	25	35	43	67
as		14.36	49.30	24.35	33.21	24.40	62.95
pval		1.34%	29.00%	1.84%	0.00%	0.00%	0.00%
v_{max}		7.39e−2	2.57e−1	2.20e−1	–	–	–
$\bar{v}$		1.52e−2	5.72e−2	7.60e−2	–	–	–
umin	LPS-1	1.70e−1	2.61e−2	9.83e−2	6.91e−3	6.01e−1	1.73e−1
	LPS-2	1.72e−1	2.64e−2	1.10e−1	7.73e−3	6.00e−1	1.78e−1
	LPS-3	9.98e−2	4.86e−2	−2.52e−1	7.68e−4	1.31e−1	−3.34e−2
umax	LPS-1	1.7494	1.8450	1.9050	1.9889	1.8527	1.8294
	LPS-2	1.7477	1.8318	1.9063	1.9865	1.8511	1.8242
	LPS-3	1.8594	2.0779	2.1922	2.0107	2.0460	1.9953
$L_2 - error$ order	LPS-1	1.82	1.47	0.56	1.75	1.77	1.48
	LPS-2	1.81	1.39	0.55	1.76	1.77	1.53
	LPS-3	1.93	2.06	1.38	2.06	1.99	2.05
$H_1 - error$ order	LPS-1	0.87	0.80	0.30	1.48	1.34	0.81
	LPS-2	0.85	0.74	0.30	1.42	1.36	0.76
	LPS-3	0.96	1.48	0.96	1.58	1.43	1.13

Table 5
Numerical results for Λ_3 on all six mesh types.

Item	Scheme	Mesh B	Mesh C	Mesh D	Mesh F	Mesh H	Mesh I
umin	LPS-1	3.58e−2	2.52e−2	6.99e−4	7.96e−4	1.14e−1	9.07e−2
	LPS-2	3.59e−2	−1.71e−2	6.99e−4	7.44e−4	1.11e−1	8.64e−2
	LPS-3	4.12e−3	3.46e−2	−3.92e−3	5.93e−4	1.15e−1	1.11e−1
umax	LPS-1	0.7721	0.8663	0.9990	0.9953	0.8739	0.8401
	LPS-2	0.8593	0.9442	0.9997	0.9953	0.8567	0.8112
	LPS-3	1.0479	1.0811	1.2283	1.0242	1.0601	1.0384
$L_2 - error$ order	LPS-1	1.15	1.93	2.14	2.11	2.19	–
	LPS-2	0.77	1.81	2.21	2.12	2.12	–
	LPS-3	1.66	1.99	2.00	2.14	2.22	2.56
$H_1 - error$ order	LPS-1	0.63	1.61	1.19	2.11	1.61	–
	LPS-2	0.12	0.75	1.36	2.15	1.64	–
	LPS-3	0.71	1.32	1.27	2.38	1.68	1.49

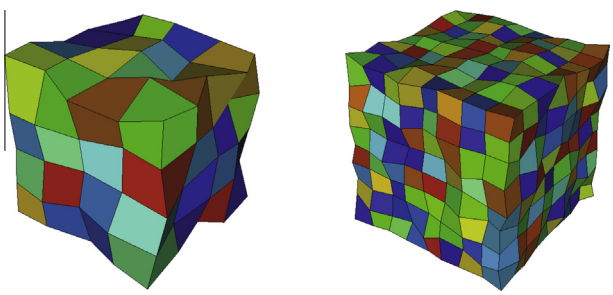

Fig. 4. Mesh AA_1(left) and Mesh AA_2(right).

$$\Lambda_4 = \begin{cases} \mathrm{diag}(1,1,1), & y \leqslant 0.5, \\ \begin{pmatrix} a & 1 & 1 \\ 1 & a & 1 \\ 1 & 1 & a \end{pmatrix}, & y > 0.5 \end{cases}$$

and

$$u_3(x,y,z) = \begin{cases} x+y+z+b(y-0.5)^2 e^{x+y+z}, & y \leqslant 0.5, \\ x-\frac{y}{a}+z+\frac{1+a}{2a}+b(y-0.5)^2 e^{x+y+z}, & y > 0.5, \end{cases}$$

Table 6
Numerical results for Λ_2 and randomly disturbed hexahedral meshes.

Item	Scheme	Mesh AA_1	Mesh AA_2	Mesh AA_3	Mesh AA_4
nunkw		64	512	4096	32768
ms		22	25	25	25
as		15.25	19.94	22.42	23.70
pval		30.00%	38.89%	44.12%	46.97%
v_{max}		8.69e−2	1.09e−1	1.36e−1	1.34e−1
$\bar{v}$		2.72e−2	2.59e−2	2.46e−2	2.41e−2
umin	LPS-1	1.07e−2	3.88e−4	2.45e−4	1.08e−6
	LPS-2	1.07e−2	5.21e−4	2.39e−4	−1.96e−6
	LPS-3	1.07e−2	1.21e−3	1.30e−4	4.57e−6
umax	LPS-1	0.9534	0.9810	0.9984	0.9989
	LPS-2	0.9676	0.9848	0.9990	0.9985
	LPS-3	0.9050	0.9907	0.9931	0.9985
$L_2 - error$	LPS-1	2.21e−2	6.26e−3	1.68e−3	4.52e−4
	LPS-2	2.41e−2	6.43e−3	1.55e−3	3.93e−4
	LPS-3	1.84e−2	4.68e−3	1.35e−3	3.37e−4
$H_1 - error$	LPS-1	2.57e−1	1.36e−1	7.26e−2	3.89e−2
	LPS-2	2.90e−1	1.44e−1	6.42e−2	3.26e−2
	LPS-3	1.91e−1	1.08e−1	5.84e−2	3.02e−2

Table 7
Numerical results for Λ_3 and randomly disturbed hexahedral meshes.

Item	Scheme	Mesh AA_1	Mesh AA_2	Mesh AA_3	Mesh AA_4
	LPS-1	1.06e−2	2.40e−4	2.17e−4	1.69e−6
umin	LPS-2	1.06e−2	3.74e−4	2.10e−4	−1.43e−6
	LPS-3	1.06e−2	1.19e−3	1.27e−4	4.10e−6
umax	LPS-1	0.9534	0.9806	1.0003	0.9992
	LPS-2	0.9684	0.9848	1.0011	0.9985
	LPS-3	0.9013	0.9900	0.9928	0.9985
$L_2 - error$	LPS-1	2.29e−2	6.94e−3	2.20e−3	7.40e−4
	LPS-2	2.50e−2	7.07e−3	1.92e−3	5.97e−4
	LPS-3	1.93e−2	4.81e−3	1.40e−3	3.51e−4
$H_1 - error$	LPS-1	2.65e−1	1.51e−1	9.71e−2	6.40e−2
	LPS-2	3.00e−1	1.58e−1	8.00e−2	4.91e−2
	LPS-3	1.95e−1	1.09e−1	5.96e−2	3.08e−2

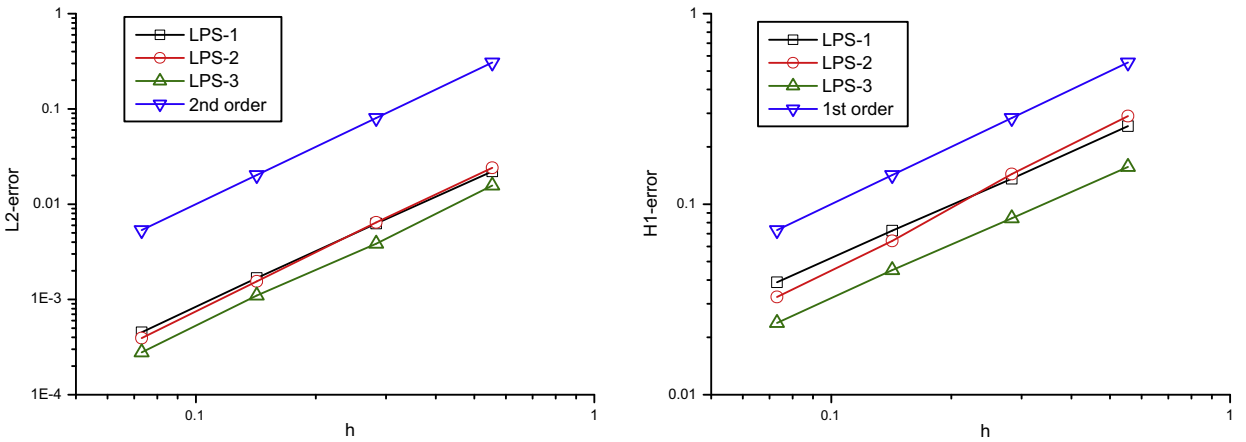

Fig. 5. Test 2: errors for Λ_2 on randomly disturbed hexahedral meshes.

respectively, where a, b are two constants. Obviously, the diffusion tensor changes the eigenvalues and orientations of eigenvectors across the plane $y = 0.5$. The source function f are determined by the diffusion Eq. (2.1), Λ_4 and u_3. The meshes adopted here are similar to the ones used in Test 2 except that the vertices on the plane $y = 0.5$ are not allowed to move in the $y-$direction. More explicitly, the coordinates of the randomly disturbed hexahedral meshes are given by

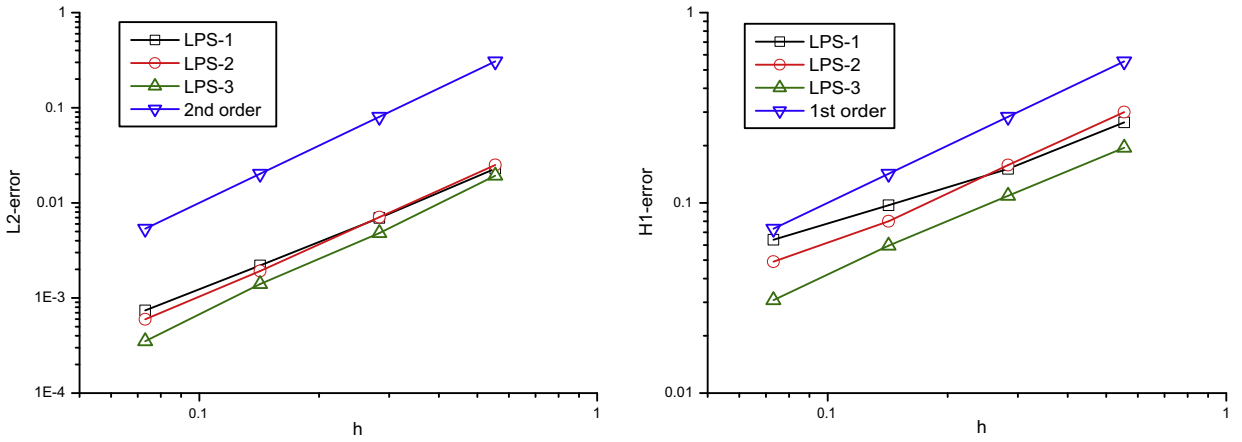

Fig. 6. Test 2: errors for Λ_3 on randomly disturbed hexahedral meshes.

Table 8
Numerical results for Λ_4 and randomly disturbed hexahedral meshes.

Item	Scheme	$N=4$	$N=8$	$N=16$	$N=32$	$N=64$
nunkw		64	512	4096	32768	262144
$L_2-error$	LPS-1	6.23e−2	2.47e−2	7.42e−3	1.96e−3	5.50e−4
	LPS-2	6.54e−2	2.47e−2	7.49e−3	2.05e−3	7.59e−4
	LPS-3	4.73e−2	2.02e−2	5.74e−3	1.64e−3	4.17e−4
$H_1-error$	LPS-1	7.23e−1	4.05e−1	2.10e−1	8.82e−2	4.85e−2
	LPS-2	7.65e−1	4.05e−1	2.14e−1	1.01e−1	7.67e−2
	LPS-3	4.45e−1	3.11e−1	1.65e−1	8.93e−2	4.72e−2

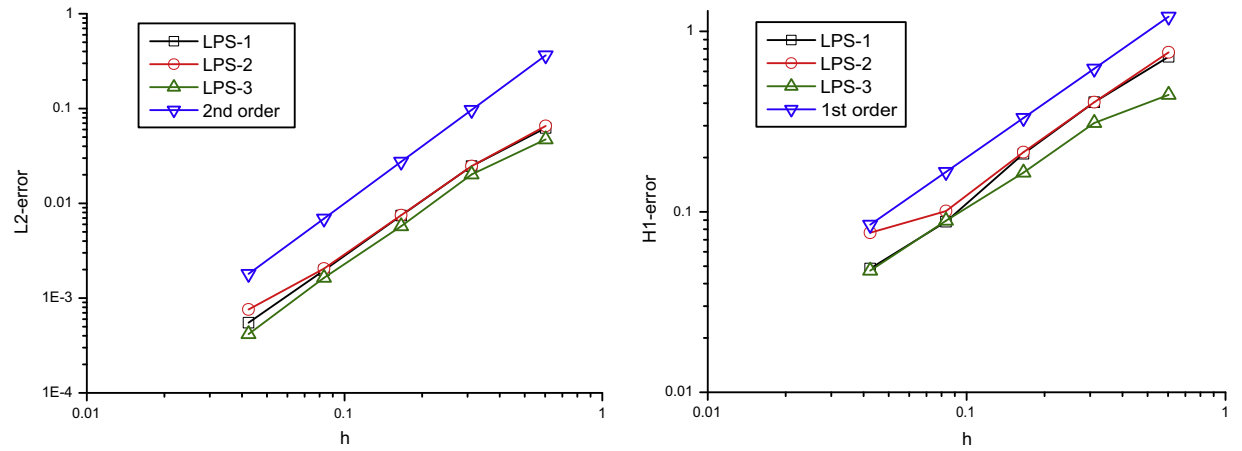

Fig. 7. Test 3: errors for Λ_4 on randomly disturbed hexahedral meshes.

$$x_i = \frac{i}{N} + c_1 r_1 h', \quad y_j = \frac{j}{N} + c_2 r_2 h', \quad z_k = \frac{k}{N} + c_3 r_3 h', \quad 0 \leqslant i,j,k \leqslant N,$$

where $r_1,\ r_2,\ r_3 \in [-1,1]$ are three random numbers, N is a positive integer, $h' = 1/N, c_1, c_2$ and c_3 are some constants and $c_2 = 0$ if $j/N = 0.5$. This test, a modified version from the discontinuous problem in [13], is designed to investigate the linearity-preserving property and other numerical properties of the schemes when a certain discontinuous and anisotropic diffusion tensor is presented.

First, we consider a linear case where $a = 2$ and $b = 0$. For the undetermined mesh parameters, we set $c_1 = c_2 = c_3 = 0.2$ so that **(A1)**, **(A2)** and (**A2**′) are guaranteed. Still, we split any non-planar quadrilateral facet into two triangular facets. As

expected, three schemes provide the exact solution in this case, which verifies that these schemes are linearity-preserving if assumptions **(A1)**, **(A2)** and (**A2′**) are satisfied.

Secondly, we choose $a = 2,\ b = 1$ and $c_1 = c_2 = c_3 = 0.3$. In this case, the solution is not piecewise linear and moreover, the meshes have a larger distortion than the above linearity-preserving test so that **(A1)** or **(A2)** may not be satisfied. The results for `nunkw`, `ms`, `as`, `pval`, v_{max} and $\bar{v}$ are almost the same as those in Table 6 so that they are not shown. Other detailed results are presented in Table 8 and the errors are also shown graphically in Fig. 7. We can see that the numerical performance of the schemes is very good in this test.

References

[1] I. Aavatsmark, An introduction to multipoint flux approximations for quadrilateral grids, Comput. Geosci. 6 (3–4) (2002) 405–432.
[2] L. Agelas, R. Eymard, R. Herbin, A nine-point finite volume scheme for the simulation of diffusion in heterogeneous media, C.R. Acad. Sci. Paris, Ser. I 347 (11–12) (2009) 673–676.
[3] B. Andreianov, F. Boyer, F. Hubert, Discrete duality finite volume schemes for Leray-Lions-type elliptic problems on general 2D meshes, Numer. Methods Partial Differ. Equ. 23 (1) (2007) 145–195.
[4] F. Brezzi, K. Lipnikov, V. Simoncini, A family of mimetic finite difference methods on polygonal and polyhedral meshes, Math. Models Methods Appl. Sci. 15 (10) (2005) 1533–1551.
[5] F. Brezzi, K. Lipnikov, M. Shashkov, V. Simoncini, A new discretization methodology for diffusion problems on generalized polyhedral meshes, Comput. Methods Appl. Mech. Engrg. 196 (37–40) (2007) 3682–3692.
[6] Q. Chen, J. Wan, Y. Yang, R. Mifflin, Enriched multi-point flux approximation for general grids, J. Comput. Phys. 227 (3) (2008) 1701–1721.
[7] Y. Coudiére, J.-P. Vila, P. Villedieu, Convergence rate of a finite volume scheme for a two-dimensional diffusion convection problem, Math. Model. Numer. Anal. 33 (3) (1999) 493–516.
[8] Y. Coudiére, C. Pierre, O. Rousseau, R. Turpault, A 2D/3D discrete duality finite volume scheme. Application to ECG simulation, Int. J. Finite 6 (1) (2009) 1–24.
[9] Y. Coudiére, F. Hubert, A 3D discrete duality finite volume method for nonlinear elliptic equations, SIAM J. Sci. Comput. 33 (4) (2011) 1739–1764.
[10] S. Delcourte, K. Domelevo, P. Omnes, A discrete duality finite volume approach to Hodge decomposition and div-curl problems on almost arbitrary two-dimensional meshes, SIAM J. Numer. Anal. 45 (3) (2007) 1142–1174.
[11] M.G. Edwards, Unstructured, control-volume distributed, full-tensor finite-volume schemes with flow based grids, Comput. Geosci. 6 (3–4) (2002) 433–452.
[12] R. Eymard, G. Henry, R. Herbin, F. Hubert, R. Klöfkorn, G. Manzini, 3D benchmark on discretization schemes for anisotropic diffusion problems on general grids, in: J. Fort, J. Furst, J. Halama, R. Herbin, F. Hubert (Eds.), Finite Volumes for Complex Applications VI - Problems and Perspectives, Springer, 2011, pp. 893–929.
[13] R. Eymard, R. Herbin, C. Guichard, Small-stencil 3D schemes for diffusive flows in porous media, ESAIM Math. Model. Numer. Anal. 46 (2) (2012) 265–290.
[14] R. Eymard, T. Gallouët, R. Herbin, Discretization of heterogeneous and anisotropic diffusion problems on general nonconforming meshes SUSHI: a scheme using stabilization and hybrid interfaces, IMA J. Numer. Anal. 30 (4) (2010) 1009–1043.
[15] Z. Gao, J. Wu, A linearity-preserving cell-centered scheme for the heterogeneous and anisotropic diffusion equations on general meshes, Int. J. Numer. Methods in Fluids 67 (12) (2011) 2157–2183.
[16] X. Hang, W. Sun, C. Ye, Finite volume solution of heat and moisture transfer through three-dimensional textile materials, Comput. Fluids 57 (2012) 25–39.
[17] R. Herbin, F. Hubert, Benchmark on discretization schemes for anisotropic diffusion problems on general grids, in: R. Eymard, J.M. Herard (Eds.), Finite Volumes for Complex Applications (V), Wiley, 2008, pp. 659–692.
[18] F. Hermeline, Approximation of diffusion operators with discontinuous tensor coefficients on distorted meshes, Comput. Methods Appl. Mech. Engrg. 192 (16–18) (2003) 1939–1959.
[19] F. Hermeline, Approximation of 2-D and 3-D diffusion operators with variable full tensor coefficients on arbitrary meshes, Comput. Methods Appl. Mech. Engrg. 196 (21–24) (2007) 2497–2526.
[20] F. Hermeline, A finite volume method for approximating 3D diffusion operators on general meshes, J. Comput. Phys. 228 (16) (2009) 5763–5786.
[21] R.A. Klausen, R. Winther, Robust convergence of multi point flux approximation on rough grids, Numer. Math. 104 (3) (2006) 317–337.
[22] B. Li, W. Sun, Heat-sweat flow in three-dimensional porous textile media, Nonlinearity 25 (2) (2012) 421–447.
[23] K. Lipnikov, M. Shashkov, I. Yotov, Local flux mimetic finite difference methods, Numer. Math. 112 (1) (2009) 115–152.
[24] K. Lipnikov, D. Svyatskiy, Y. Vassilevski, Interpolation-free monotone finite volume method for diffusion equations on polygonal meshes, J. Comput. Phys. 228 (3) (2009) 703–716.
[25] M.F. Wheeler, I. Yotov, A multipoint flux mixed finite element method, SIAM J. Numer. Anal. 44 (5) (2006) 2082–2106.
[26] J. Wu, Z. Dai, Z. Gao, G. Yuan, Linearity preserving nine-point schemes for diffusion equation on distorted quadrilateral meshes, J. Comput. Phys. 229 (9) (2010) 3382–3401.
[27] J. Wu, Z. Gao, A nine-point scheme with explicit weights for diffusion equations on distorted meshes, Appl. Numer. Math. 61 (7) (2011) 844–867.
[28] J. Wu, Z. Gao, Z. Dai, A stabilized linearity-preserving scheme for the heterogeneous and anisotropic diffusion problems on polygonal meshes, J. Comput. Phys. 231 (21) (2012) 7152–7169.
[29] G. Yuan, Z. Sheng, Monotone finite volume schemes for diffusion equations on polygonal meshes, J. Comput. Phys. 227 (12) (2008) 6288–6312.
[30] Q. Zhao, G. Yuan, Analysis and construction of cell-centered finite volume scheme for diffusion equations on distorted meshes, Comput. Methods Appl. Mech. Engrg. 198 (34–40) (2009) 3039–3050.